J Nanostruct 15(4): 1844-1859, Autumn 2025

RESEARCH PAPER

Physiochemical Characterization of Hydroxyapatite Nanoparticle-Modified Mineral Trioxide Aggregate and Bioceramic Sealers

Arkhawan Ali Abdulhaq [1], Chenar Anwar Mohammad [1], Bassam Karim Amin [2]*

[1] *Department of periodontic, College of Dentistry, Hawler Medical University, Erbil, Kurdistan Region, Iraq*
[2] *Department of Conservative, College of Dentistry, Hawler Medical University, Erbil, Kurdistan Region, Iraq*

ARTICLE INFO

Article History:
Received 04 July 2025
Accepted 25 September 2025
Published 01 October 2025

Keywords:
Bioceramic sealer
FTIR
Hydroxyapatite nanoparticles
Mineral trioxide aggregate
SEM

ABSTRACT

Hydroxyapatite nanoparticle (HANP) incorporation into dental biomaterials is a promising approach that may help improve their nanostructure, chemical stability, and bioactivity. In the present work the mineral trioxide aggregate (MTA) and premixed bioceramic (BC) sealer were adjusted with HANP, in the proportion of 2, 4, and 6 by weight and systematically characterized by Fourier transform infrared spectroscopy (FTIR), scanning electron microscopy (SEM), and energy-dispersive X-ray spectroscopy (EDS). FTIR proved successful incorporation of HANP without modifying the primary functional groups of the sealers. The morphological variations demonstrated by SEM were concentration-dependent: partial nanoparticle cluster, uniform dispersion with maximized nano-roughness, and agglomeration with minimal functional surface activity were observed with 2, 4, and 6 percent HANP, respectively. Elemental mapping identified Ca, P, and O and Ca/P ratios indicated that they were clearly dependent on the HANP content. The formulation of HANP (4 %) gave Ca/P ratios closest to the stoichiometric ratio of hydroxyapatite (1.67), whereas 6 % HANP was very different suggesting that it contained calcium rich domains and had low potential bioactivity. These findings reveal that moderation of HANP concentration (4%) optimizes nanostructure, elemental components, and physicochemical characteristics of MTA and BC sealers, which points to its suitability in enhancing osteoconductivity and mineralization in clinical practice.

How to cite this article
Abdulhaq A., Mohammad C., Amin B. Physiochemical Characterization of Hydroxyapatite Nanoparticle-Modified Mineral Trioxide Aggregate and Bioceramic Sealers . J Nanostruct, 2025; 15(4):1844-1859. DOI: 10.22052/JNS.2025.04.032

INTRODUCTION

Root canal sealers are used to provide a seal between the dentinal walls and the filling material along the entire length of the root canal. Ideally, these cements should have sealing ability, dimensional stability, adequate setting time, insolubility, and biocompatibility, given the risk of material extrusion beyond the apical constriction and direct contact with periapical tissues [1]. Because of their exceptional sealing capabilities, high biocompatibility, and ability to encourage periapical healing through hard tissue creation, mineral trioxide aggregate (MTA) and bioceramic (BC) sealers are frequently utilized in endodontic therapy [2]. MTA, composed primarily of tricalcium silicate, dicalcium silicate and bismuth

* *Corresponding Author Email: arkhawan.ali@hmu.edu.krd*

oxide, has shown superior biological performance, but has limitations such as handling difficulties and a prolonged setting time [3]. bioceramic sealers (BC) sealers have good physicochemical qualities and enhanced clinical usability, although more improvement in their mechanical strength and bioactivity is still preferred [4, 5]. Enhancing dental materials using nanotechnology has shown promise, especially when it comes to adding nanoparticles to sealers to increase their physical, chemical, and biological qualities [6]. Hydroxyapatite have been incorporated into root canal sealers, retrofilling materials, dental composites and adhesive resin systems to enhance the mechanical, physicochemical and biological properties of materials. Nanohydroxyapatite (HANP) is considered a biocompatible and bioactive material and presents osteoconductive properties [7]. Among these, the nanosized HA has an ultrafine nanostructure with less than 100 nm grain size in at least one direction. It precisely mimics the physiochemical composition of the natural bone minerals and shows enhanced resorbability and bioactivity. Furthermore, the release of calcium ions from the nanocrystalline HA is faster than in coarser crystals. Thus, bioceramics based on nanosized HA is a material of choice for various biomedical applications because of improved mechanical properties, sinterability, densification, cellular attachment, proliferation, and differentiation [8]. It has been demonstrated that HANP incorporation into dental materials such as adhesives, glass ionomer cements, and sealers alters surface shape, ion release profiles, and setting behavior—elements crucial for enhancing clinical results [9, 10].

Although numerous studies have investigated the incorporation of HANP into various dental materials, including adhesives and sealers, most have focused primarily on biological properties or antibacterial effects, with limited attention given to detailed physicochemical characterization. To date, no comparative studies have systematically evaluated the impact of different HANP concentrations on both MTA and BC sealers using comprehensive analytical methods. Therefore, this study aims to fill this gap by assessing the physicochemical changes resulting from the incorporation of HANP at concentrations of 2%, 4%, and 6% by weight into MTA and BC sealers. Using detailed analytical methods—including Fourier transform infrared spectroscopy (FTIR), scanning electron microscopy (SEM), and energy dispersive X-ray spectroscopy (EDX)—this study seeks to establish foundational insights into the structural and compositional characteristics of HANP-modified sealers, thus informing their potential clinical application and guiding further in vivo research.

MATERIALS AND METHODS

Preparation of modified sealer with hydroxyapatite nanoparticle

Hydroxyapatite nanoparticles (HANP) in the present study were obtained commercially from (MERK, GERMANY). Incorporation technique was used for HANP mixing with bioceramic (ONE-FIL bioceramic sealer, MEDICLUS CO., LTD. Korea) and mineral trioxide aggregate MTA (MTA Cem, NEXOBIO Co., Korea) sealers.

procedure

Three different concentrations (2%, 4%, and 6%) of HANP were carefully weighed using an analytical balance, and each was combined separately with 1 g of MTA and BC sealer. For the MTA groups, the HANP powder was initially mixed thoroughly with MTA powder using a vortex mixer (LP vortex mixer, Thermos Scientific, USA), with the powder enclosed in a disposable tube and vigorously mixed for one minute [11], Subsequently, distilled water was added to the HANP-MTA mixture on a glass plate and mixed using a metal spatula according to the manufacturer's instructions [12]. For the BC groups, each HANP concentration was incorporated directly into 1 g of pre-mixed BC sealer. The HANP and BC were manually blended on a clean glass slab using a sterile stainless-steel spatula until achieving a homogeneous paste, which was then transferred into a disposable tube. To enhance dispersion and minimize agglomeration of nanoparticles, the tube was placed into a bath sonicator with a holder and sonicated for 30 minutes at room temperature [13, 14]. The overall preparation sequence is illustrated in Fig. 1.

Nanoparticle characterization

Different sample tests were used to characterize HANP, MTA-modified with HANP and BC-modified with HANP in different ways such as scanning electron microscope (SEM) (FESEM model MIRA3, TESCAN; JAPAN) to identify surface morphology. Energy dispersive spectroscopy (EDX) (FESEM model MIRA3, TESCAN; JAPAN) was used for

elemental analysis and Fourier transform infrared spectroscopy (FTIR: MODEL Spectrum TWO Perkin Elmer) to confirm and identify functional groups present in both pure nanoparticle and the mixture [5, 15-17].

RESULTS AND DISCUSSION

Fourier transform infrared spectroscopy (FTIR) of MTA, HANP and MTA modified with HANP

The analysis process of FTIR remains popular for functional group detection across pure components and combined substances alongside compound comparison studies. This analytical method depends on the fundamental link between atoms and molecules while they vibrate [18]. The (FTIR) spectroscopy of MTA, HANP and MTA-HANP were shown in Fig. 2.

The FTIR spectrum of MTA revealed the presence of several important functional groups. The presence of the stretching vibration band

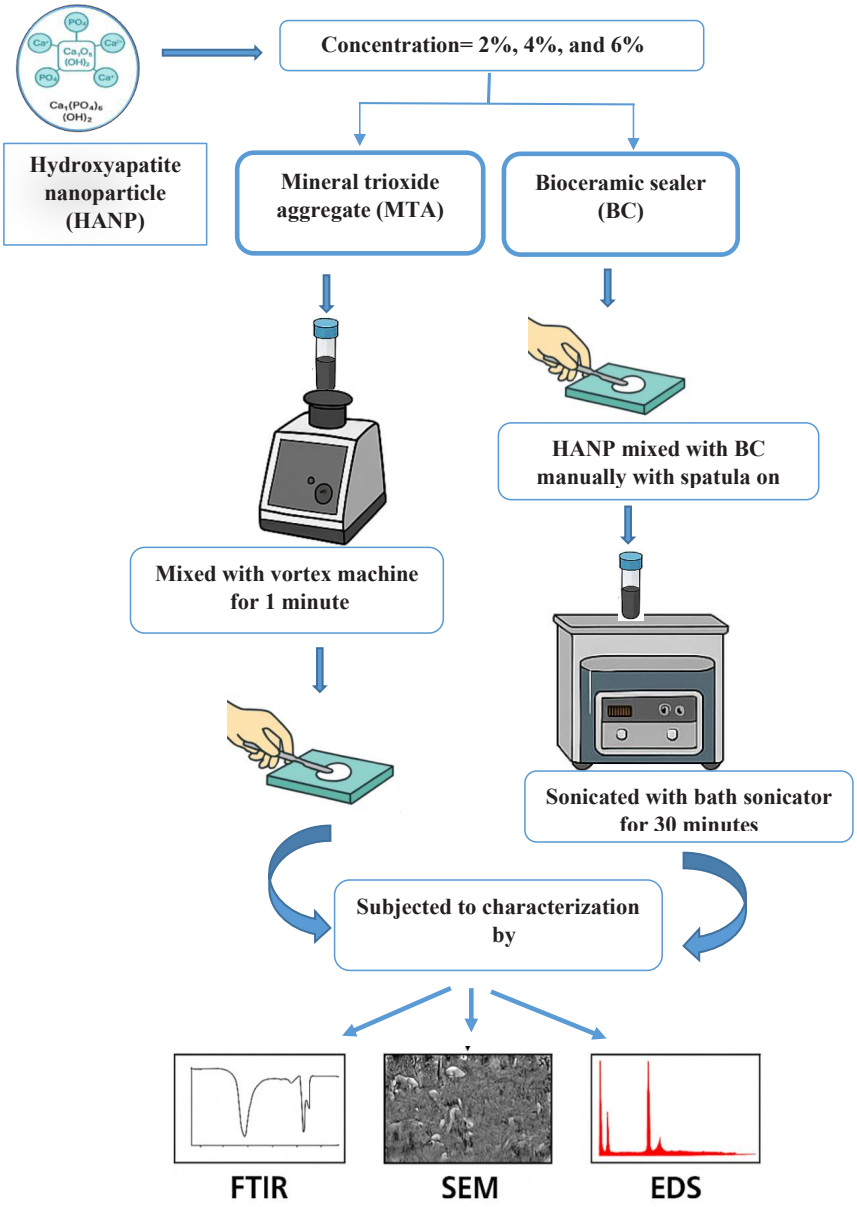

Fig. 1. Schematic diagram of mixing different concentrations of HANP with both MTA and BC.

at 2367.37 cm^{-1} correspond to C-H, while the stretching band at 3434.98 cm^{-1} is indicated by the presence of hydroxyl groups. Furthermore, the inorganic components of MTA are reflected by peaks in the lower wavenumber region (520, 48 cm^{-1}), correspond to a silicate or phosphate-based structures. this result is in accordance with previous studies by [19-21].

The FTIR spectra of hydroxyapatite nanoparticle showed two strong absorption bands at 1037.05 cm^{-1} and 564.29 cm^{-1}, which are attributed to $PO4^{-1}$ and a weak absorption at 3432.80 corresponding to the hydroxyle group as illustrated by [22-24].

All vibration peaks identified in the FTIR spectra of MTA- modified with HANP, are included in the FTIR spectrum of the finished product (MTA-HANP). Both MTA and hydroxyapatite frequently exhibit structural hydroxyl groups and adsorbed water, which are reflected in the broad absorption band at around 3434 cm^{-1}, which corresponds to the O–H stretching vibration. The C–H stretching vibration is responsible for the band located at 2367 cm^{-1}. Significant peaks in the lower wavenumber range, including those at 946 cm^{-1}, 602 cm^{-1}, and 520 cm^{-1}, are ascribed to silicate (Si–O) and phosphate (P–O) stretching modes. These peaks are compatible with the calcium silicate matrix of MTA and the composition of HANP. According to these results, HANP was successfully added to MTA to improve its bioactive phosphate profile without compromising its structural integrity. This finding is in line with researches by [19, 25].

Fourier transform infrared spectroscopy (FTIR) of BC, HANP and BC-modified with HANP

The FTIR spectra of the bioceramic (BC) sealer revealed a high absorption band at 2881 cm^{-1}, which is associated with the C-H stretching vibration band, and a stretching band at 3558 cm^{-1}, which is associated with the hydroxyl O-H group. the lower wavenumbers at 526.67 cm^{-1} and 946.21 cm^{-1} suggest the inorganic silicate, Si-O (Silicon-Oxygen) bond, or phosphate-based components commonly seen in bioceramic materials. Our result is Consistent with findings from other previous investigations [26-28].

All of the vibration peaks found in the FTIR spectra of BC and HANP are present in the FTIR spectrum of the finished product (BC-HANP) without changing any physiochemical or mechanical properties demonstrating that the nanoparticles were successfully integrated. The O–H stretching vibration is linked to a broad band at 3557 cm^{-1}, which reflects the structural hydroxyl groups and hydrogen bonding that are commonly found in hydrated bioceramic and hydroxapatite systems. The existence of organic components is shown by the C–H stretching-corresponding absorption at 2881 cm^{-1}. Strong phosphate-related

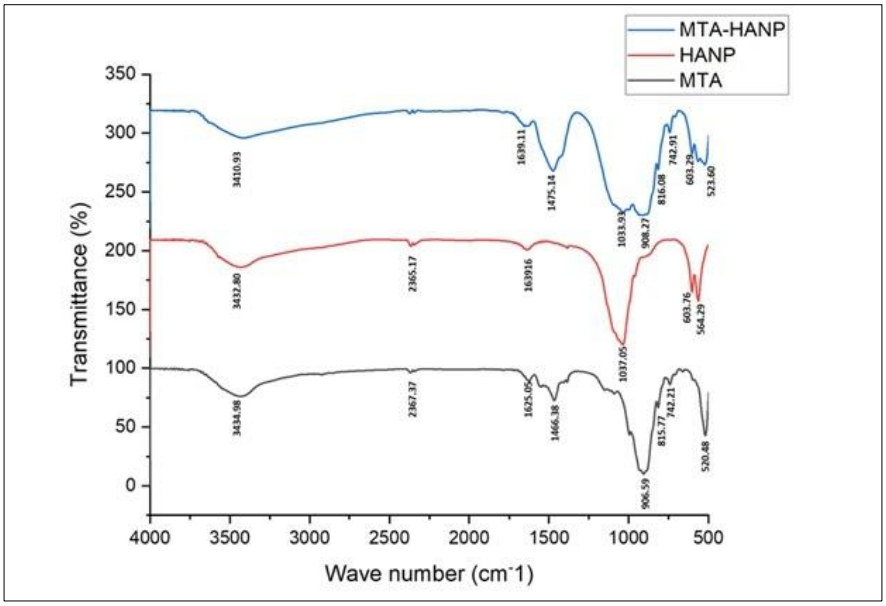

Fig. 2. FTIR spectra of pure MTA, pure HANP, and MTA modified with HANP (MTA-HANP).

peaks that are consistent with PO_4^{3-} bending and stretching modes of hydroxyapatite can be seen at 946.29 cm^{-1}, 564.29 cm^{-1}, and 522.67 cm^{-1}.This is consistent with the results of Baghdadi et al., who found that the stability and synergy of the composite were demonstrated by the preservation of the distinctive FTIR peaks of both components, including the O–H, C–H, and phosphate group

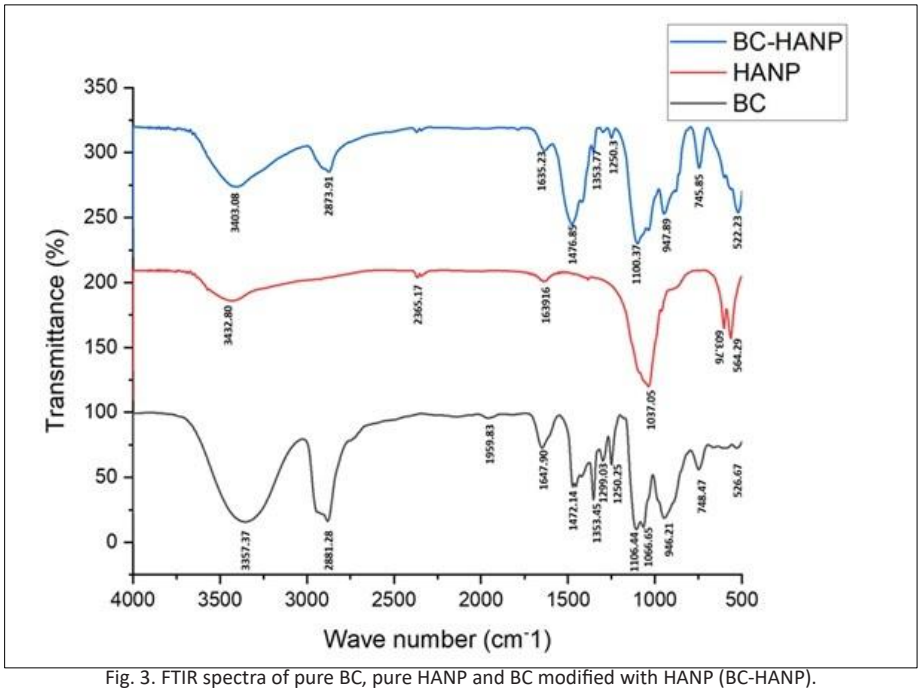

Fig. 3. FTIR spectra of pure BC, pure HANP and BC modified with HANP (BC-HANP).

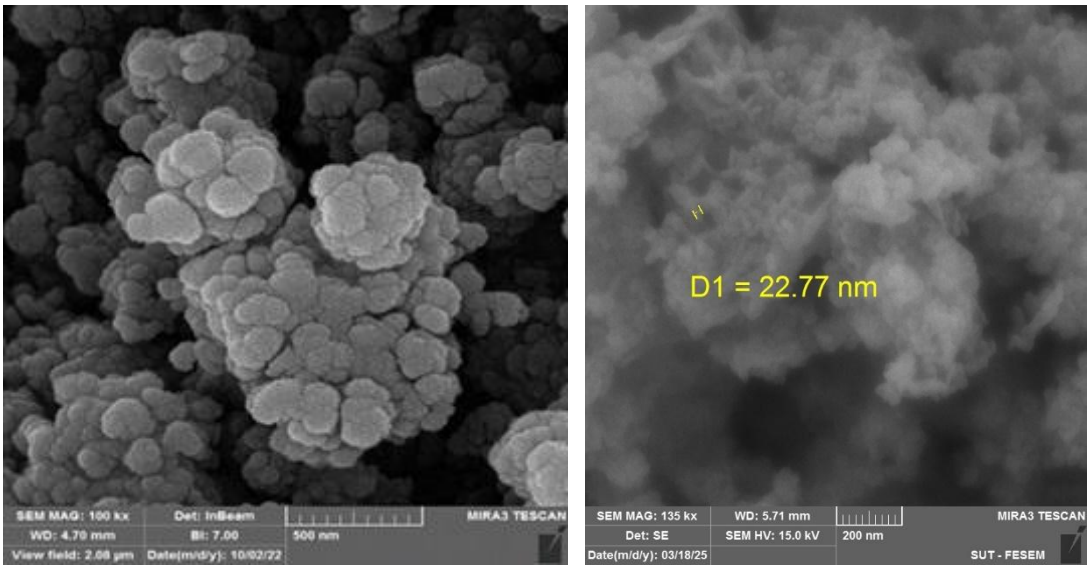

A B

Fig. 4. SEM characterization of pure HANP: (A) Particle size distribution at high magnification (FESEM); (B) Morphology showing spherical nanoparticles and agglomerates.

bands, when bioactive nanomaterials like hydroxyapatite added to bioceramic sealers [29]. Similarly, Abu-Zaid et al., found that HA-reinforced sealers preserved the hydroxyl and silicate structure and showed phosphate bands between 560 and 1030 cm^{-1}, improving the material's mineralisation potential and biocompatibility [30]. The FTIR spectrum of BC, HANP and BC-modified with HANP were shown in Fig. 3.

Scanning electron microscope (SEM) of pure hydroxyapatite nanoparticles

The morphology of HANP was examined in the current study using a scanning electron

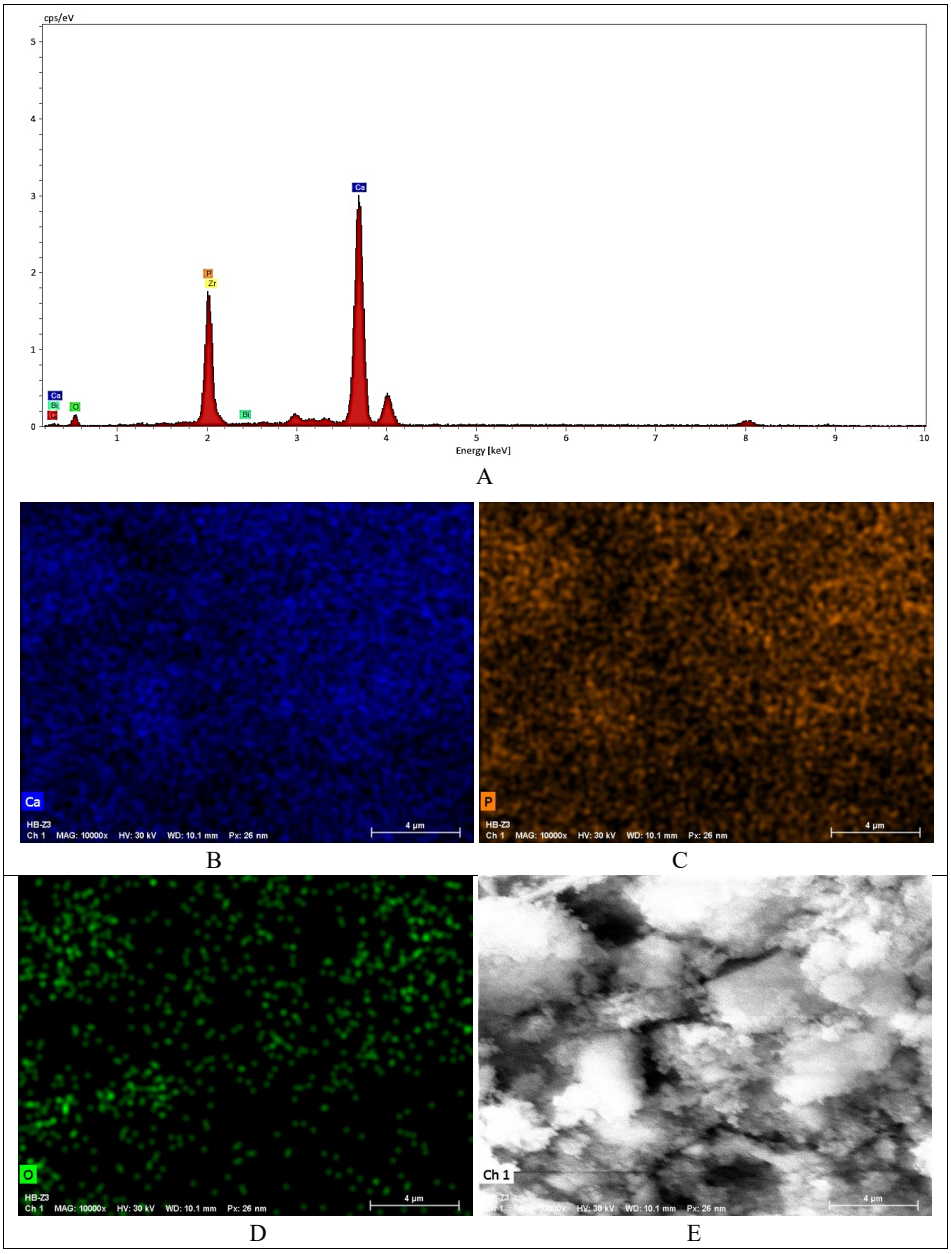

Fig. 5. EDX and elemental mapping (MAPS) of pure HANP: (A) EDX spectrum confirming elemental composition; Elemental distribution maps of (B) Oxygen (O), (C) Phosphorus (P), and (D) Calcium (Ca); (E) SEM image showing area analyzed by EDX.

microscope both before and after incorporation of HANP in to sealers. The HANP were found to be spherical by SEM analysis, with an average particle size range of 20.98-39.55 nm, as shown in Fig. 4A. A few isolated particles and mostly agglomerated HANP were visible in the SEM pictures. The nanoparticles showed no signs of sharp edges, as illustrated in Fig. 4B, this result was in accordance with previous studies by [9, 31, 32].

Energy dispersive x-ray spectroscopy (EDX) and MAPS characterizations of pure hydroxyapatite nanoparticles (HANP)

EDX analysis identified calcium (Ca), oxygen (O), phosphorus (P), and carbon (C) as the primary elements in HANP shown in Fig. 5 A. Elemental mapping (MAPS) revealed uniform distributions of oxygen, phosphorus, and calcium across the nanoparticle surfaces [31]. The detailed EDX spectrum Fig. 5B-E

confirmed the purity and characteristic composition of the synthesized HANP.

Scanning electron microscope (SEM) of mineral trioxide aggregate (MTA)

The SEM analysis of MTA at 5000×showed heterogeneous microstructure as shown in Fig. 6., which characterized by irregularly shaped particles and a porous topology. This morphology is consistent with recent studies, which have documented that particle size of MTA in microscale have structural inequality, Multiple aggregates of big, spherical particles with an elongated form have been found, as presented by [33-35].

Energy dispersive x-ray spectroscopy and MAPS characterization of mineral trioxide aggregate (MTA)

Elemental analysis of pure MTA showed identical distributions for elements which included Ca, O, Si, Al, and C. All significant peaks detected during EDS analysis involved calcium, silicon, aluminum, bismuth along with oxygen as presented by [36].

The elemental composition of MTA sample was analyzed using EDS was shown in Fig. 7A. The result revealed that calcium (Ca) and Oxygen (O) were predominant, with weight percentage of (39.23) % and (37.80) %, respectively, indicating the presence of calcium-rich phases such as calcium silicate and oxides. Silicon (Si) was also detected at (8.06), supporting the existence of silicate compound integral to the cement matrix. Minor constituents included aluminum (AI) (2.07) %, sulfur (S) (1.31) % and bismuth (Bi) (3.10%), corresponding to possible inclusion of alumina, calcium sulfate, and bismuth oxide, respectively. Ytterbium was also present at (8.42) %, which incorporated as radioopacifier. Unlike Gandolfi'

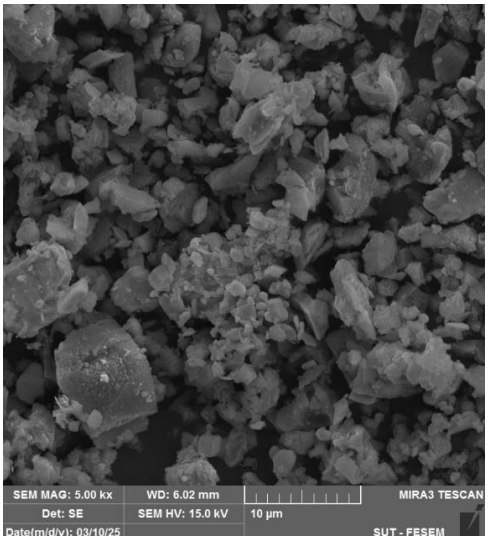

Fig. 6. FESEM micrograph illustrating the surface morphology of pure MTA powder at 5000× magnification, revealing irregularly shaped particles and porous structures.

study, Our research yielded no Cl [37].

Scanning electron microscope of bioceramic sealer (BC)

SEM examination of the pure BC sealer surface at 1500× magnification revealed moderately dense, irregularly shaped particles embedded within a partially porous structure as presented in Fig. 8. The surface displayed a mixture of smooth and granular areas interspersed with micropores

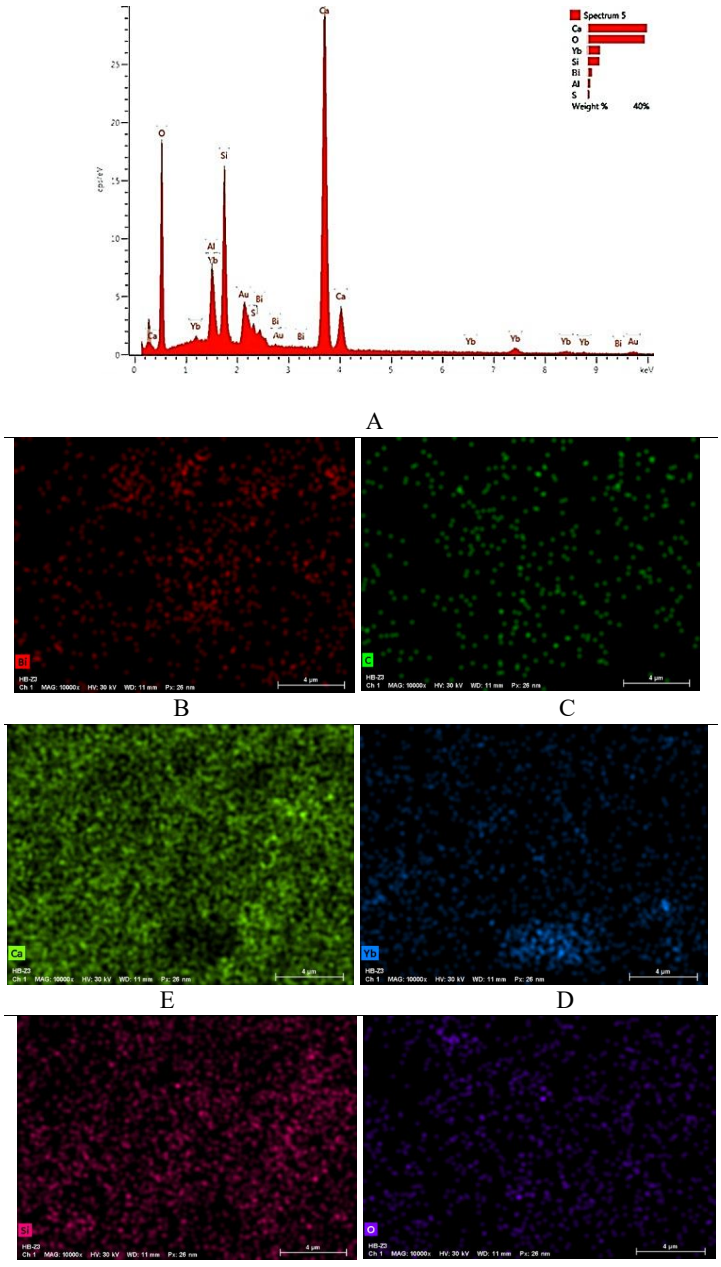

Fig. 7. EDX analysis and elemental mapping of pure MTA: (A) EDX spectrum; Elemental distribution maps for (B) Bismuth (Bi), (C) Carbon (C), (D) Calcium (Ca), (E) Ytterbium (Yb), (F) Silicon (Si), and (G) Oxygen (O).

distributed unevenly throughout the sample. Other studies' findings supported the surface's appearance of both smooth and granular regions as well as indications of microporous structures dispersed unevenly throughout the field [38-40].

Energy dispersive x-ray spectroscopy and MAPS characterization of bioceramic sealer

Fig. 9B–G shows EDS analysis of the pure BC sealer demonstrated prominent elemental peaks of carbon (C), oxygen (O), zirconium (Zr), calcium (Ca), silicon (Si), aluminum (Al), and minor gold (Au) from surface coating (Fig. 9A). Quantitative measurements indicated oxygen (29.48%) and zirconium (12.99%) as major constituents, followed by calcium (7.40%), silicon (1.35%), and aluminum (0.41%). Carbon was present at the highest proportion (48.73%). Elemental distribution maps (MAPS) highlighted uniform spatial distribution of these elements throughout the sample. This elemental makeup is in good agreement with findings in calcium silicate-based sealers that have been previously published [4, 41].

Scanning electron microscope of MTA-modified with HANP

SEM images of MTA modified with the HANP at the concentrations of 2, 4, and 6 percent, which were taken at the magnification of 5,000x, were shown in Fig. 10 A-C. demonstrated the significant changes of the surface morphology and the distribution of nanoparticles. The MTA-modified MTA with HANP' surface shape and nanoparticle dispersion showed distinct concentration-dependent patterns, according to the SEM data. The sealer showed large, flaky crystalline formations with observable aggregation of nanoparticles at 2% HANP, indicating inadequate integration. A more uniform particle distribution, decreased porosity, and improved interparticle contact were the results of increasing HANP to 4%, which produced optimal dispersion and was consistent with research showing that moderate HANP loading supports structural integrity and sufficient surface area exposure necessary for bioactivity. According to our SEM data, 4% HANP integration resulted in ideal nano-roughness and

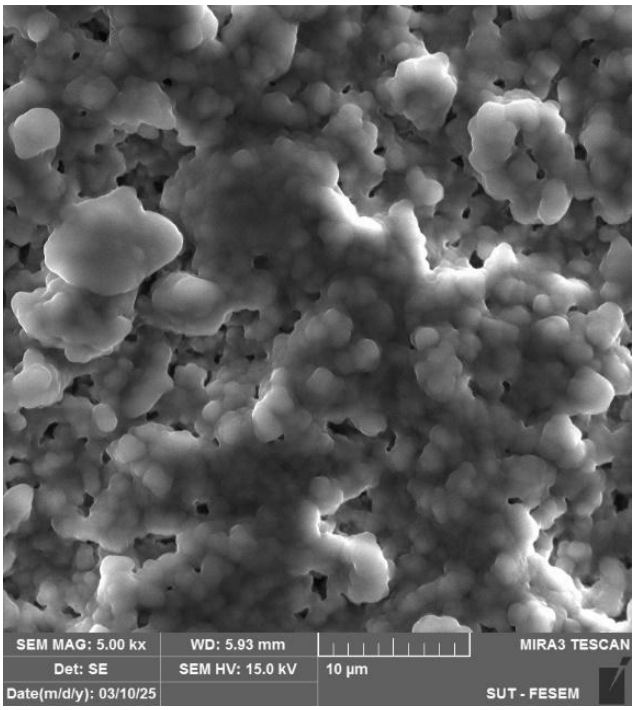

Fig. 8. Surface morphology characterization of pure BC sealer at 1500× magnification demonstrating particle distribution.

homogenous nanoparticle dispersion, which are associated with improved mineralization and osteoblast interactions. Dhavalikar et al. (2023) published similar results, showing that human mesenchymal stem cells (hMSC) vitality was enhanced by nanoparticle coverage at pore surfaces [42].

However, raising HANP to 6% likely resulted in larger clusters and smoother surfaces due to nanoparticle saturation and agglomeration, which

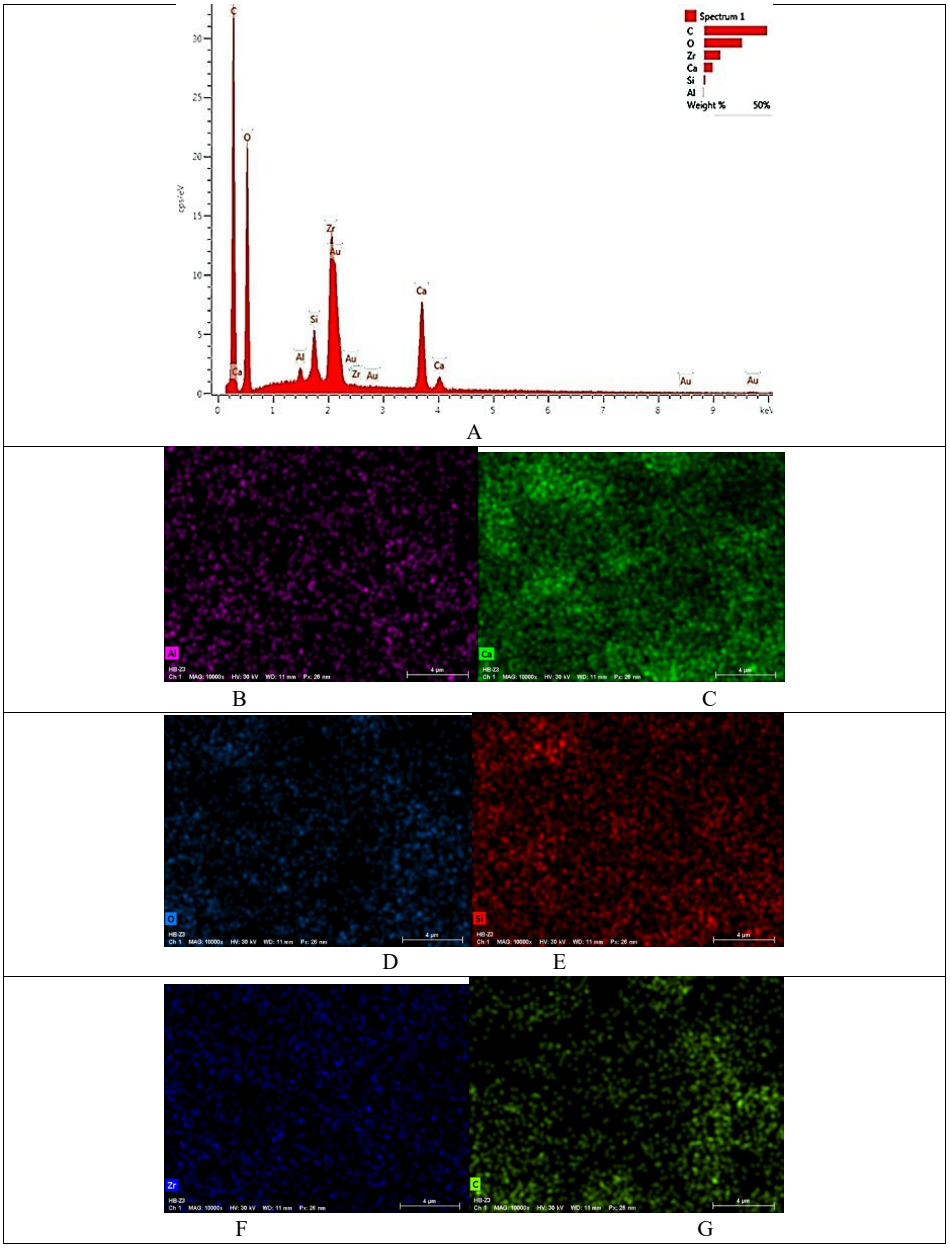

Fig. 9. EDX spectrum and elemental mapping of pure BC sealer: (A) EDX spectrum confirming elemental composition; Elemental maps illustrating distribution of (B) Aluminum (Al), (C) Calcium (Ca), (D) Oxygen (O), (E) Silicon (Si), (F) Zirconium (Zr), and (G) Carbon (C).

is known to limit functional surface activity and diminish specific surface area, altering and losing their nano-properties. The most difficult issue these studies encountered when integrating the nanoparticles with the dental materials was their propensity to aggregate. These findings are in line with earlier research that demonstrated that the best possible nanoparticle dispersion is necessary for functional composite performance, — Not too low to be ineffectual, nor too high to cause a reinforcing fall and not distributed well within the martials [43, 44].

Scanning electron microscope of BC-modified with HANP

In the SEM analysis conducted on modified BC sealers with HANP, various degrees of concentration were observed to have distinct

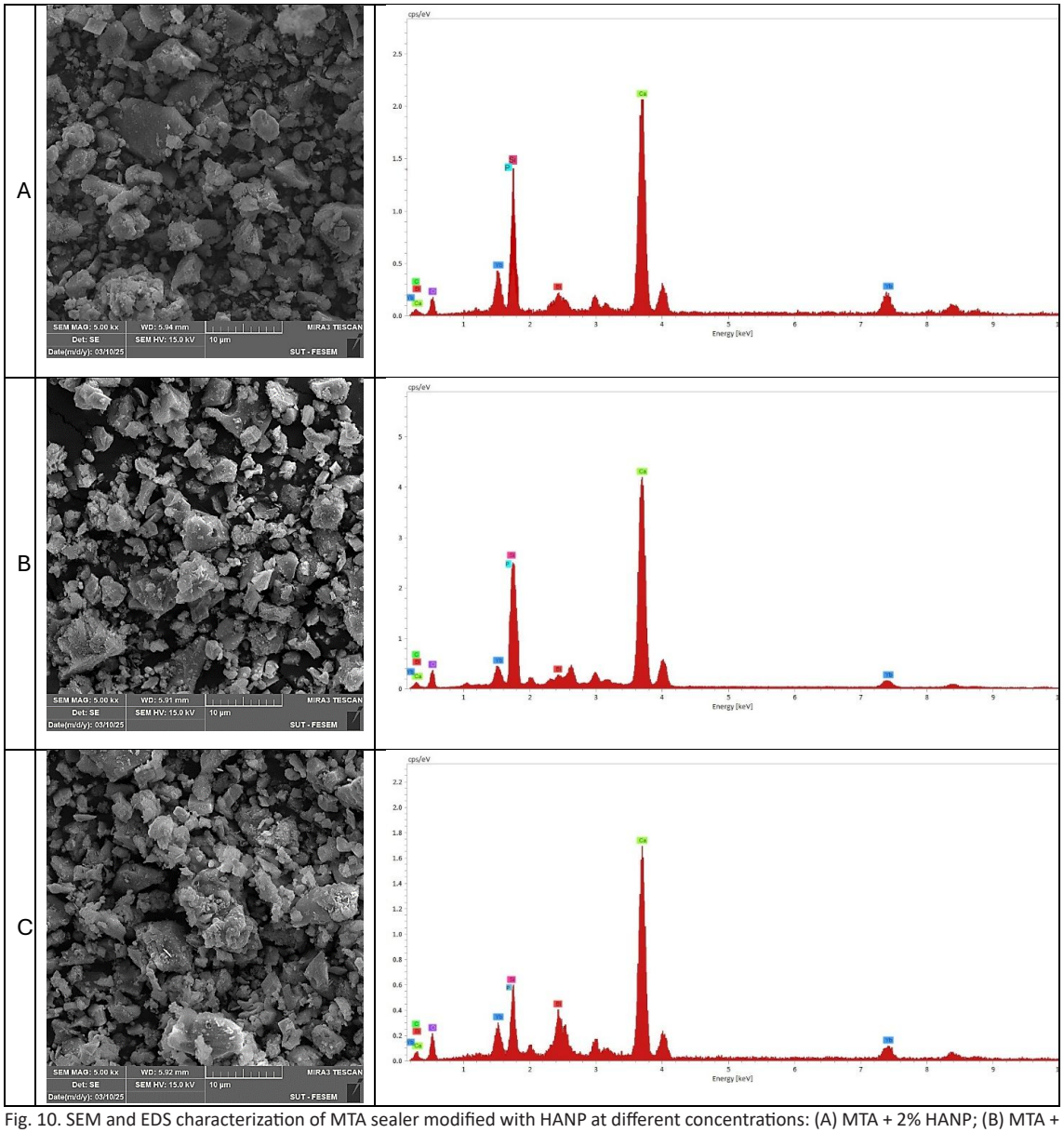

Fig. 10. SEM and EDS characterization of MTA sealer modified with HANP at different concentrations: (A) MTA + 2% HANP; (B) MTA + 4% HANP; (C) MTA + 6% HANP. Images highlight improvements in nanoparticle integration and surface homogeneity at the optimal concentration (4%).

differences in the surface morphology of the sealers. When the concentration of HANP was 2%, the surface was relatively smooth and the distribution of nanoparticles became very even. At higher concentration (4%), slightly rougher surfaces were observed and the homogeneity of the nanoparticle was improved. At the highest concentration where the particles were examined (6%), the strong agglomeration of nanoparticles and the rise of roughness were examined. This behaviour is consistent with the previous findings by [45]. Similarly, Sari et al. (2021) found that as

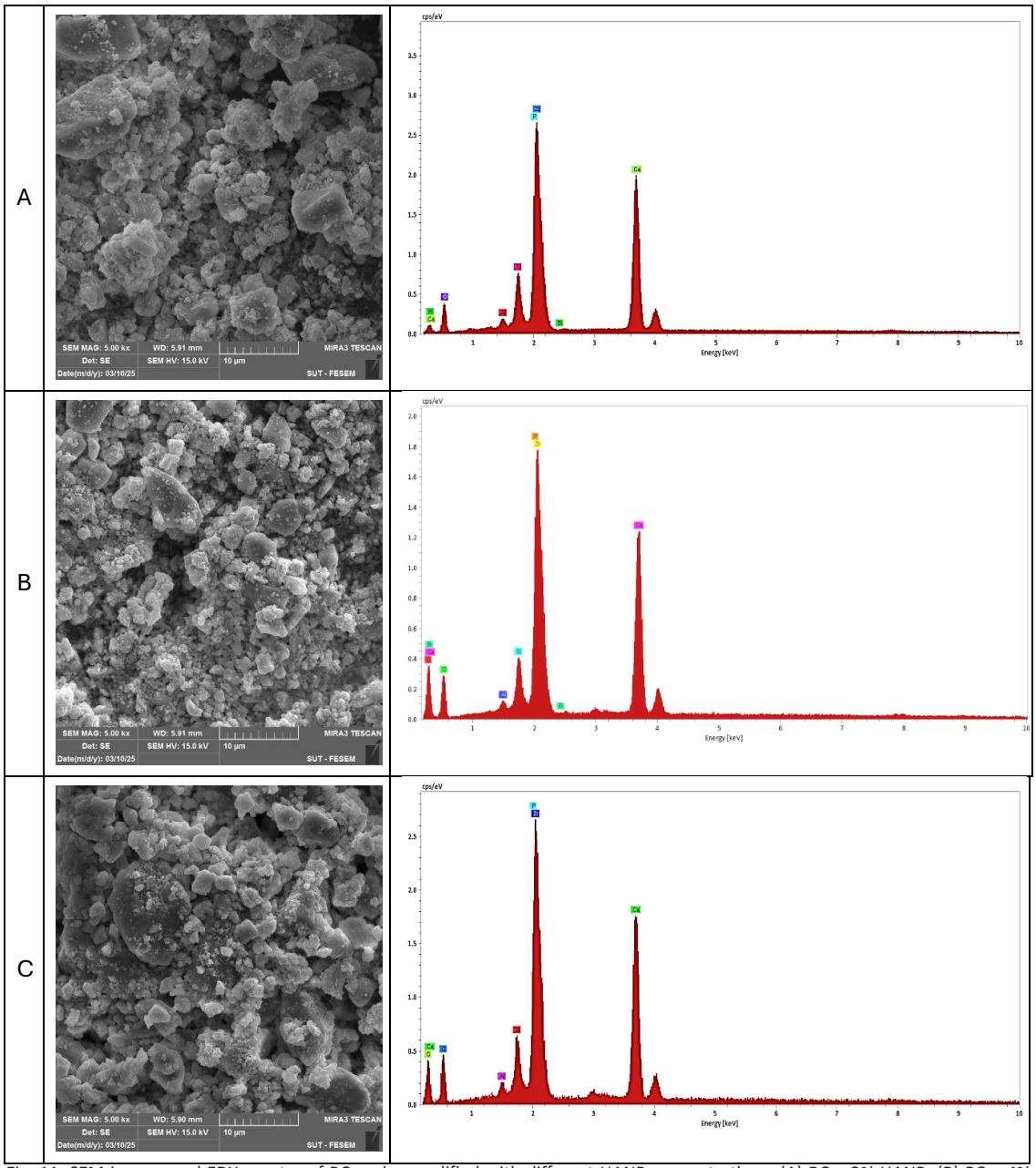

Fig. 11. SEM images and EDX spectra of BC sealer modified with different HANP concentrations: (A) BC + 2% HANP; (B) BC + 4% HANP; (C) BC + 6% HANP. Micrographs illustrate nanoparticle dispersion and surface morphology changes with increasing HANP content.

the HANP content in bioceramic scaffolds grew, porosity and surface roughness increased as well, they attributed this to matrix saturation and nanoparticle clustering [46]. The representative

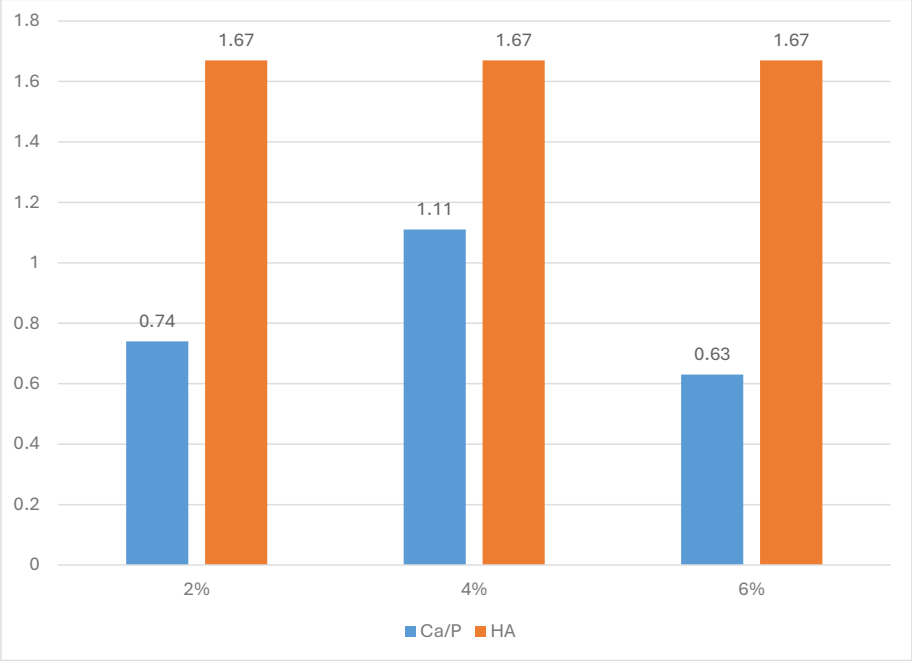

Fig. 13. The Ca/P ratio from EDS microanalysis of the BC.

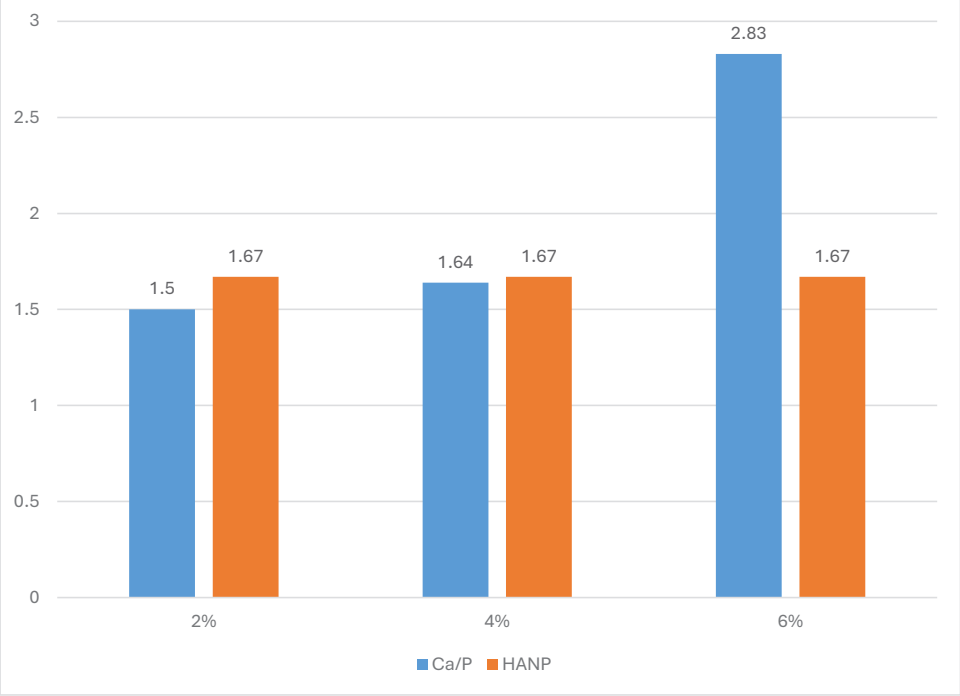

Fig. 12. The Ca/P ratio from EDS microanalysis of the MTA.

SEM images that support these morphological trends can be seen in Fig. 11A-C.

Energy dispersive spectroscopy BC- modified with HANP and MTA- modified with HANP

As the EDS analysis indicated, the HANP-modified MTA and BC sealers contained calcium (Ca), phosphorus (P) and oxygen (O) thus indicating that an addition of the nanoparticle was effective. The rise in Ca/P was found to be associated with increase in the levels of HANP. The presence of hydroxyapatite nanoparticles in the mixture is indicated by the detection of these components as presented by [5, 32, 47]. Typical EDS spectra were displayed in Figs. 10 and 11.

Calcium to phosphate CA/P ratio of HANP-modified MTA and BC

Mineral Trioxide Aggregate (MTA) and Bioceramic sealers (BC) were subjected to energy-dispersive X-ray spectroscopy (EDS) microanalysis to assess the Ca/P ratios of the two materials when different concentrations of hydroxyapatite nanoparticles (HANP) were added (2, 4 and 6% concentrations) Figs. 12. and 13. There was a concentration-dependent trends in both materials. The Ca/P ratios at 2 % HANP were also slightly elevated relative to controls, which suggests partial improvement of calcium over phosphorus. Adding 4 percent HANP yielded Ca/P ratios nearest to the stoichiometric ratio of hydroxyapatite (1.67), a standard that exhibits optimal physicochemical stability and bone-like characteristics [48, 49]. But further addition of HANP to 6 % resulted in a significant absence of this ideal ratio, which suggests an imbalance that may be related to nanoparticle agglomeration or uneven distribution. The Ca/P stoichiometry of 1.67 in hydroxyapatite is close to natural bone mineral, however, and appears to be a desirable target when it comes to regenerating of bones by biomaterials [50]. Bioactivities above this value, which can be observed in the 6 % HANP groups, can reflect calcium-rich phases that might decrease bioactivity or change resorption behavior [51]. Past research on hydroxyapatite bioceramics has also reported that processing conditions, purity of the phases, and crystallinity have a major effect on the Ca/P ratio and, consequently, the bioactivity of the final product (Hammood et al. 2019). Past research on hydroxyapatite bioceramics has also reported that processing conditions, purity of the phases, and crystallinity have a major effect on the Ca/P ratio and, consequently, the bioactivity of the final product [52].

The balance obtained at 4 % HANP indicates that this concentration reflects an optimum incorporation level that improves the physicochemical profile of MTA and BC without causing a compositional imbalance.

CONCLUSION

Nanostructural and physicochemical properties characterizing hydroxyapatite nanoparticles modified sealers showed a definite dependence on the nanoparticle concentration. Addition of 4% HANP led to uniformity, desirable nano-topography, and Ca/P ratios that were almost similar with the stoichiometric value of 1.67, thus improving the bone-like structure of MTA and BC sealers. Conversely, incorporation of 6 % HANP facilitated the formation of agglomeration and calcium-rich phases; these could hamper the bioactivity of the material. These in vitro results should be confirmed by future work with biological experiments and in vivo studies to determine long-term regenerative effects.

ACKNOWLEDGMENT

The author appreciates the encouragement and support given by the Department of Periodontics, College of Dentistry, Hawler Medical University. Thanks belong to the laboratory staff members who were involved in the process of providing technical assistance.

CONFLICT OF INTEREST

The authors declare that there is no conflict of interests regarding the publication of this manuscript.

REFERENCES

1. Paz JER, Costa PO, Souza AAC, Oliveira IMd, Falcão LF, Falcão CAM, et al. Bone repair in defects filled with AH Plus sealer and different concentrations of MTA: a study in rat tibiae. Restorative Dentistry and Endodontics. 2021;46(4).
2. Estivalet MS, de Araújo LP, Immich F, da Silva AF, Ferreira NdS, da Rosa WLdO, et al. Bioactivity Potential of Bioceramic-Based Root Canal Sealers: A Scoping Review. Life. 2022;12(11):1853.
3. Abu Zeid ST, Edrees HY. Hydration Characterization of Two Generations of MTA-Based Root Canal Sealers. Applied Sciences. 2022;12(7):3517.
4. Radwanski M, Piwonski I, Szmechtyk T, Sauro S, Lukomska-Szymanska M. Microstructural and Elemental Characterization of Calcium Silicate-Based Sealers. Nanomaterials. 2025;15(10):756.
5. Almutairi B, Alkhudhairy F. Nanoparticles modified bioceramic sealers on solubility, antimicrobial efficacy, pushout bond

strength and marginal adaptation at apical-third of canal dentin. PeerJ. 2025;13:e18840.
6. Pushpalatha C, Gayathri VS, Sowmya SV, Augustine D, Alamoudi A, Zidane B, et al. Nanohydroxyapatite in dentistry: A comprehensive review. The Saudi Dental Journal. 2023;35(6):741-752.
7. Guerreiro-Tanomaru JM, VÁZquez-GarcÍA FA, Bosso-Martelo R, Bernardi MIB, Faria G, Tanomaru Filho M. Effect of addition of nano-hydroxyapatite on physico-chemical and antibiofilm properties of calcium silicate cements. Journal of Applied Oral Science. 2016;24(3):204-210.
8. Khan I, Saeed K, Khan I. Nanoparticles: Properties, applications and toxicities. Arabian Journal of Chemistry. 2019;12(7):908-931.
9. Al-Hamdan RS, Almutairi B, Kattan HF, Alresayes S, Abduljabbar T, Vohra F. Assessment of Hydroxyapatite Nanospheres Incorporated Dentin Adhesive. A SEM/EDX, Micro-Raman, Microtensile and Micro-Indentation Study. Coatings. 2020;10(12):1181.
10. Ilancheran P, Paulraj J, Maiti S, Shanmugam R. Green Synthesis, Characterization, and Evaluation of the Antimicrobial Properties and Compressive Strength of Hydroxyapatite Nanoparticle-Incorporated Glass Ionomer Cement. Cureus. 2024.
11. Genaro LE, Anovazzi G, Hebling J, Zuanon ACC. Glass Ionomer Cement Modified by Resin with Incorporation of Nanohydroxyapatite: In Vitro Evaluation of Physical-Biological Properties. Nanomaterials. 2020;10(7):1412.
12. Bichile M, Mahaparale R, Mattigatti S, Wahane K, Raut S. Push-out bond strength of mineral trioxide aggregate with addition of titanium dioxide, silver, and silicon dioxide nanoparticles: An in vitro comparative study. Journal of Conservative Dentistry. 2022;25(5):541.
13. . European Journal of Educational Research. 2024;volume-13-2024(volume-13-issue-3-july-2024).
14. Zanghellini B, Knaack P, Schörpf S, Semlitsch K-H, Lichtenegger HC, Praher B, et al. Solvent-Free Ultrasonic Dispersion of Nanofillers in Epoxy Matrix. Polymers. 2021;13(2):308.
15. Aljamhan AS, Alrefeai MH, Alhabdan A, Alhusseini SA, Farooq I, Vohra F, et al. Influence of ER-CR-YSGG Laser and Photodynamic Therapy on the Dentin Bond Integrity of Nano-Hydroxyapatite Containing Resin Dentin Adhesive: SEM-EDX, Micro-Raman, Micro-Tensile, and FTIR Evaluation. Polymers. 2021;13(12):1903.
16. Omar K. Tin Oxide Nanoparticles: Synthesis, Characterization and Study their Particle Size at Different Current Density. ARO, The Scientific Journal of Koya University. 2013:17-21.
17. Rajeshkumar S, Jeevitha M. Plant-mediated biosynthesis and characterization of zinc oxide nanoparticles. Zinc-Based Nanostructures for Environmental and Agricultural Applications: Elsevier; 2021. p. 37-51. http://dx.doi.org/10.1016/b978-0-12-822836-4.00023-9
18. A Comprehensive Review of Nanomaterials: Types, Synthesis, Characterization, and Applications. Biointerface Research in Applied Chemistry. 2022;13(1):41.
19. Bolhari B, Chitsaz N, Nazari S, Behroozibakhsh M, Sooratgar A, Hashemian A. Effect of Fluorohydroxyapatite on Biological and Physical Properties of MTA Angelus. The Scientific World Journal. 2023;2023:1-8.
20. Ahmed MS, Hasan NH, Saeed MG. Chemical analysis of mineral trioxide agregate mixed with hyaluronic acids as an accelerant. Brazilian Dental Journal. 2023;34(6):50-66.
21. Nguyen NT, Nguyen VA. Ultrasound-assisted sol-gel synthesis, characterization, and photocatalytic application of ZnO nanoparticles. Digest Journal of Nanomaterials and Biostructures. 2023;18(3):889-897.
22. Pereyra M, Navatta M, Méndez E. Failure in the adhesion of hydroxyapatite coatings to surgical screws: a fourier transform infrared spectroscopy qualitative study. Frontiers in Coatings, Dyes and Interface Engineering. 2025;3.
23. Zanca C, Patella B, Capuana E, Lopresti F, Brucato V, Carfi Pavia F, et al. Behavior of Calcium Phosphate–Chitosan–Collagen Composite Coating on AISI 304 for Orthopedic Applications. Polymers. 2022;14(23):5108.
24. Rafie S, Nordin D. Synthesis and Characterization 0f Hydroxyapatite Nanoparticle. Malaysian Journal of Analytical Science. 2017;21(1):136-148.
25. Barros CMB, de Oliveira SV, Marques JB, de Souto Viana KM, de Melo Costa ACF. Analysis of the Hydroxyapatite Incorporate MTA Dental Application. Mater Sci Forum. 2012;727-728:1381-1386.
26. Nagdi AH, Mokhless NA, Aboelseoud MR. Evaluation of the tubular penetration of two different types of nanoparticle root canal sealers over apically separated files: a scanning electron microscopic study (in vitro study). BMC Oral Health. 2025;25(1).
27. Kim H-I, Jang Y-E, Kim Y, Kim BS. Physicochemical Changes in Root-Canal Sealers under Thermal Challenge: A Comparative Analysis of Calcium Silicate- and Epoxy-Resin-Based Sealers. Materials. 2024;17(8):1932.
28. Lin GSS, Sim DHH, Luddin N, Lai JCH, Ghani HA, Noorani TY. Fabrication and characterisation of novel algin incorporated bioactive-glass 58S calcium-silicate-based root canal sealer. Journal of Dental Sciences. 2023;18(2):604-612.
29. Baghdadi I, Zaazou A, Tarboush BA, Zakhour M, Özcan M, Salameh Z. Physiochemical properties of a bioceramic-based root canal sealer reinforced with multi-walled carbon nanotubes, titanium carbide and boron nitride biomaterials. Journal of the Mechanical Behavior of Biomedical Materials. 2020;110:103892.
30. Abu-Zeid ST, Saif RE, Mostafa HA, Edrees HY. Characterization and Crystallinity of Two Bioactive Sealers: Qualitative and Quantitative Analysis. Applied Sciences. 2024;14(3):1285.
31. Bahra HA, Niaz Hamaghareeb H, Faiq HSH. Novel incorporation of charged hydroxyapatite nanoparticles into resin adhesive. Cell Mol Biol. 2023;69(11):149-154.
32. Jerri Al-Bakhsh BA, Shafiei F, Hashemian A, Shekofteh K, Bolhari B, Behroozibakhsh M. In-vitro bioactivity evaluation and physical properties of an epoxy-based dental sealer reinforced with synthesized fluorine-substituted hydroxyapatite, hydroxyapatite and bioactive glass nanofillers. Bioactive Materials. 2019;4:322-333.
33. Jo BW, Chakraborty S, Yoon KW. Synthesis of a Cementitious Material Nanocement Using Bottom-Up Nanotechnology Concept: An Alternative Approach to Avoid CO_2 Emission during Production of Cement. Journal of Nanomaterials. 2014;2014(1).
34. Mahmoud O, Al-Afifi NA, Salihu Farook M, Ibrahim MA, Al Shehadat S, Alsaegh MA. Morphological and Chemical Analysis of Different Types of Calcium Silicate-Based Cements. International Journal of Dentistry. 2022;2022(1).
35. Chang SW. Chemical Composition and Porosity Characteristics of Various Calcium Silicate-Based Endodontic Cements. Bioinorganic Chemistry and Applications. 2018;2018:1-6.
36. Zarra T, Lambrianidis T, Vasiliadis L, Gogos C. Effect of curing conditions on physical and chemical properties of MTA+.

International Endodontic Journal. 2018;51(11):1279-1291.
37. Gandolfi MG, Van Landuyt K, Taddei P, Modena E, Van Meerbeek B, Prati C. Environmental Scanning Electron Microscopy Connected with Energy Dispersive X-ray Analysis and Raman Techniques to Study ProRoot Mineral Trioxide Aggregate and Calcium Silicate Cements in Wet Conditions and in Real Time. Journal of Endodontics. 2010;36(5):851-857.
38. Raman V, Camilleri J. Characterization and Assessment of Physical Properties of 3 Single Syringe Hydraulic Cement–based Sealers. Journal of Endodontics. 2024;50(3):381-388.
39. Zamparini F, Prati C, Taddei P, Spinelli A, Di Foggia M, Gandolfi MG. Chemical-Physical Properties and Bioactivity of New Premixed Calcium Silicate-Bioceramic Root Canal Sealers. International Journal of Molecular Sciences. 2022;23(22):13914.
40. Assiry AA, Karobari MI, Lin GSS, Batul R, Snigdha NT, Luke AM, et al. Microstructural and Elemental Characterization of Root Canal Sealers Using FTIR, SEM, and EDS Analysis. Applied Sciences. 2023;13(7):4517.
41. Reszka P, Nowicka A, Lipski M, Dura W, Droździk A, Woźniak K. A Comparative Chemical Study of Calcium Silicate-Containing and Epoxy Resin-Based Root Canal Sealers. BioMed Research International. 2016;2016:1-8.
42. Dhavalikar P, Jenkins D, Rosen N, Kannapiran A, Salhadar K, Shachaf O, et al. Hydroxyapatite nanoparticle-modified porous bone grafts with improved cell attachment. Journal of Materials Chemistry B. 2023;11(44):10651-10664.
43. Naguib G, Maghrabi AA, Mira AI, Mously HA, Hajjaj M, Hamed MT. Influence of inorganic nanoparticles on dental materials' mechanical properties. A narrative review. BMC Oral Health. 2023;23(1).
44. Jandt KD, Watts DC. Nanotechnology in dentistry: Present and future perspectives on dental nanomaterials. Dent Mater. 2020;36(11):1365-1378.
45. Paulraj J, Shanmugam R, Maiti S, Ganesh S. Surface Roughness and Wettability of Green-mediated Titanium, Zirconium, and Hydroxyapatite Nanocomposite-based Glass Ionomer Cement under Toothbrushing Simulation: An In Vitro Study. International Journal of Prosthodontics and Restorative Dentistry. 2024;14(1):30-38.
46. Sari M, Hening P, Chotimah, Ana ID, Yusuf Y. Bioceramic hydroxyapatite-based scaffold with a porous structure using honeycomb as a natural polymeric Porogen for bone tissue engineering. Biomaterials Research. 2021;25(1).
47. Al-Hamdan RS, Almutairi B, Kattan HF, Alsuwailem NA, Farooq I, Vohra F, et al. Influence of Hydroxyapatite Nanospheres in Dentin Adhesive on the Dentin Bond Integrity and Degree of Conversion: A Scanning Electron Microscopy (SEM), Raman, Fourier Transform-Infrared (FTIR), and Microtensile Study. Polymers. 2020;12(12):2948.
48. Fiume E, Magnaterra G, Rahdar A, Verné E, Baino F. Hydroxyapatite for Biomedical Applications: A Short Overview. Ceramics. 2021;4(4):542-563.
49. Hou X, Zhang L, Zhou Z, Luo X, Wang T, Zhao X, et al. Calcium Phosphate-Based Biomaterials for Bone Repair. Journal of Functional Biomaterials. 2022;13(4):187.
50. de Carvalho ABG, Rahimnejad M, Oliveira RLMS, Sikder P, Saavedra GSFA, Bhaduri SB, et al. Personalized bioceramic grafts for craniomaxillofacial bone regeneration. International Journal of Oral Science. 2024;16(1).
51. Ielo I, Calabrese G, De Luca G, Conoci S. Recent Advances in Hydroxyapatite-Based Biocomposites for Bone Tissue Regeneration in Orthopedics. International Journal of Molecular Sciences. 2022;23(17):9721.
52. Hammood AS, Hassan SS, Alkhafagy MT, Jaber HL. Effect of calcination temperature on characterization of natural hydroxyapatite prepared from carp fish bones. SN Applied Sciences. 2019;1(5).